ARTICLE

# Flow and Pollutant Transport in Urban Street Canyons of Different Aspect Ratios with Ground Heating: Large-Eddy Simulation

**Xian-Xiang Li · Rex E. Britter · Leslie K. Norford · Tieh-Yong Koh · Dara Entekhabi**

**Abstract**     A validated large-eddy simulation model was employed to study the effect of the aspect ratio and ground heating on the flow and pollutant dispersion in urban street canyons. Three ground-heating intensities (neutral, weak and strong) were imposed in street canyons of aspect ratio 1, 2, and 0.5. The detailed patterns of flow, turbulence, temperature and pollutant transport were analyzed and compared. Significant changes of flow and scalar patterns were caused by ground heating in the street canyon of aspect ratio 2 and 0.5, while only the street canyon of aspect ratio 0.5 showed a change in flow regime (from wake interference flow to skimming flow). The street canyon of aspect ratio 1 does not show any significant change in the flow field. Ground heating generated strong mixing of heat and pollutant; the normalized temperature inside street canyons was approximately spatially uniform and somewhat insensitive to the aspect ratio and heating intensity. This study helps elucidate the combined effects of urban geometry and thermal stratification on the urban canyon flow and pollutant dispersion.

X.-X. Li (✉)
CENSAM, Singapore-MIT Alliance for Research and Technology, S16-05-08,
3 Science Drive 2, Singapore 117543, Singapore
e-mail: lixx@smart.mit.edu

R. E. Britter
Department of Urban Studies and Planning, Massachusetts Institute of Technology, Cambridge,
MA, USA

L. K. Norford
Department of Architecture, Massachusetts Institute of Technology, Cambridge, MA, USA

T.-Y. Koh
School of Physical and Mathematical Sciences, Nanyang Technological University,
Singapore 637371, Singapore

D. Entekhabi
Department of Civil and Environmental Engineering, Massachusetts Institute of Technology,
Cambridge, MA, USA

## 1 Introduction

With rapid urbanization and city expansion, sustainable development of the urban environment is now facing many challenges, such as the urban heat-island effect, deteriorating air quality and severe security concerns (Fernando et al. 2001; Britter and Hanna 2003; Belcher 2005). As the typical element of the urban area, the street canyon exhibits a distinct climate where microscale meteorological processes dominate (Oke 1988). These microscale meteorological processes affect not only the local air quality but also the comfort of city inhabitants (Bottema 1993), which have motivated many investigations over the past several decades of the characteristics of airflow and pollutant dispersal in urban street canyons (Vardoulakis et al. 2003; Ahmad et al. 2005; Li et al. 2006).

Located within the roughness sublayer (RSL), the flow in an urban street canyon has a strong dependence on the local urban morphology and in particular the aspect ratio (AR), defined as the building-height-to-street-width ratio (AR $= h/b$, where $h$ is the building height and $b$ is the street width; see Fig. 1). The flow inside street canyons can be classified into different flow regimes according to the aspect ratio, i.e. isolated roughness flow (IRF), wake interference flow (WIF) and skimming flow (SF) regimes (Oke 1988). Within the SF regime, different aspect ratios result in different numbers of primary recirculations in urban street canyons (Li et al. 2008, 2009). Another factor, the thermal effect (due to solar radiation, the release of stored heat, and anthropogenic heat), also has a profound impact on the flow field and therefore the pollutant dispersion in street canyons, as demonstrated by many previous studies (Nakamura and Oke 1988; Ca et al. 1995; Sini et al. 1996; Uehara et al. 2000; Kim and Baik 2001; Xie et al. 2006).
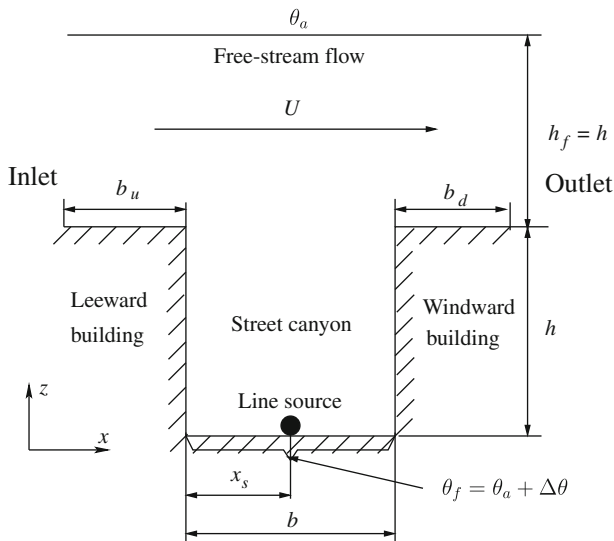


**Fig. 1** Schematic diagram of the computational domain for the flow and pollutant transport in a street canyon with ground heating

With the development of computer hardware and algorithms, the computational fluid dynamics (CFD) technique has become a popular and powerful tool in urban street-canyon research due to its efficiency and relatively low cost (Li et al. 2006). Of the many CFD models, Reynolds-averaged Navier–Stokes equations (RANS) models have provided many insights into the characteristics of the airflow and dispersion in urban street canyons (Cheng et al. 2007; Coceal et al. 2007; Hamlyn et al. 2007; Blocken et al. 2008; Reynolds and Castro 2008; Buccolieri et al. 2010). Recently, large-eddy simulation (LES) has become popular in street-canyon studies, mainly owing to its power of handling transient and unsteady turbulent processes (e.g., Liu and Barth 2002; Cui et al. 2004; Liu et al. 2004, 2005; Cai et al. 2008; Letzel et al. 2008; Li et al. 2008).

Many CFD studies, both using RANS and LES, have been performed to investigate the effects of thermal stratification in urban areas. In a series of RANS studies, Xie et al. (2005, 2006, 2007) simulated how the geometry and differential wall heating modified the flow field in an idealized two-dimensional street canyon. In addition to the aspect ratio and heat source locations, it was found that heating on the windward wall had the strongest effect on the flow field and pollutant dispersion. Xie et al. (2007) and Cheng et al. (2009) investigated the roof-level air and pollutant exchange from a street canyon with $AR = 1$ at different ground-heating intensities, and found that the square of the air exchange rate varied almost linearly with the ground-heating intensity. Kang et al. (2008) numerically investigated how flow and reactive pollutant dispersion in a street canyon with $AR = 1$ varied with the street-bottom heating intensity. The $NO$–$NO_2$–$O_3$ photochemistry was considered using a RANS model in their study. To assess the performance of turbulence models in simulating urban flow and dispersion processes, Yoshie et al. (2011) carried out CFD studies of gas and thermal dispersion behind a high-rise building in an unstable turbulent flow using RANS and LES models. Their results showed that RANS models overestimated the size of the recirculation region behind the building and underestimated the lateral dispersion of the gas. Turbulent flow structures using LES with and without inflow turbulence were completely different. More recently, the LES study by Cheng and Liu (2011) extended our understanding of the rather rarely explored scenarios of pollutant dispersion under stable stratification conditions in urban street canyons.

The LES model developed by Li et al. (2010) was validated against wind-tunnel data and then was applied to study the flow and dispersion inside the urban street canyon of $AR = 1$ with ground heating. The simulated thin thermal boundary layer near the ground agreed very well with wind-tunnel measurements (Uehara et al. 2000), which was not resolved in studies using RANS models. With different ground-heating intensities, the flow, turbulence and pollutant dispersion exhibited characteristics that were not present under isothermal conditions. In this paper, the same LES model is employed to study the combined effect of aspect ratio and ground heating on the flow pattern and thermal and pollutant dispersion in urban street canyons. The numerical model and boundary conditions are first outlined in Sect. 2, and the results of flow and turbulence fields are then described in Sect. 3. Section 4 presents and discusses the scalar fields (temperature and pollutant), and a summary is given in Sect. 5.

## 2 Numerical Model and Boundary Conditions

### 2.1 Numerical Model

The LES code (Li et al. 2010) developed for incompressible turbulent flow based on a one-equation subgrid-scale (SGS) model is employed. Using the Boussinesq approximation,

the thermal buoyancy forces are taken into account in both the dimensionless Navier–Stokes equations and the transport equation for SGS turbulent kinetic energy (TKE). The reference length scale $H$ (the building height of the street canyon of $AR = 1$), the reference velocity scale $U$ (free-stream velocity) and the reference temperature $\theta_a$ (the ambient temperature) are used to make the governing equations dimensionless. The details of the numerical model can be found elsewhere (Li 2008; Li et al. 2008, 2010) and will not be repeated here.

### 2.2 Computational Domain and Boundary Conditions

Figure 1 depicts the front view of the schematic computational domain used in the current study, which represents an idealized three-dimensional street canyon. The spanwise-homogeneous computational domain consists of a street canyon of height $h$ and a free shear layer of height $h_f = h$ above the building. The width of the street is $b$ and the length is $L$, where $L/b = 1$. The inlet and outlet length $b_u = b_d = 0.5b$. In a sensitivity test performed to justify the domain size chosen here, the free shear layer was extended to $h_f = 3h$. The results of cases with different domain sizes showed little difference in flow field patterns and averaged streamwise and vertical velocities.

The background atmospheric flow is simulated by prescribing a uniform pressure difference in the free shear layer only. The approaching airflow is perpendicular to the street axis, which results in a free-stream wind speed $U$ in the streamwise direction. The airflow boundary conditions are set to be periodic in the streamwise and spanwise directions, and no-slip conditions are set at all rigid walls. At the top of the domain, a shear-free boundary condition is assumed.

A line source of pollutant with emission rate $Q$ is located on the ground at a distance $x_s$ ($= b/2$ in this study) from the leeward building (i.e., in the middle of the street canyon). At the inlet to the computational domain, the temperature is set to $\theta_a$ and the pollutant concentration is set to zero (free of pollutant). At the outlet, the convective boundary conditions (Li et al. 2008) are prescribed for both the temperature and pollutant to ensure that they are convected outside the domain and do not re-enter the domain from the inlet. The air temperature at the top of the domain is set to the ambient temperature $\theta_a$ and the ground level (bottom) maintains a constant temperature $\theta_f = \theta_a + \Delta\theta$ (ground heating). The temperatures at the rigid walls can either be set to a fixed value (ambient temperature $\theta_a$) or adiabatic (no heat flux at walls); we take the former situation in the present study. A brief discussion of the different results of these two situations is given in Sect. 4.1.1.

### 2.3 Simulation Conditions

In this study, three street canyons of different aspect ratios, i.e., 0.5 ($h = H, b = 2H$), 1.0 ($h = b = H$) and 2.0 ($h = 2H, b = H$) are considered, and for each aspect ratio, three scenarios of ground heating (no heating, weak heating and strong heating) are investigated.

| **Table 1** Richardson numbers $Ri$ and aspect ratios $h/b$ for each case | AR | Richardson number $Ri$ | |
|---|---|---|---|
| | $h/b$ | Weak heating | Strong heating |
| | 0.5 | −0.9 | −2.9 |
| | 1.0 | −0.6 | −2.4 |
| | 2.0 | −0.5 | −2.0 |

Table 1 summarizes the conditions for all the cases studied, in which the Richardson number is defined as

$$Ri = -\frac{gh}{U^2}\frac{\Delta\theta}{\theta_{\mathrm{a}}},\tag{1}$$

where $g$ is the gravitational acceleration. The Reynolds number $Re = Uh/\nu$ for these cases varies from 4,000 to 7,000, where $\nu$ is the kinematic viscosity of air. The grid used consists of $64 \times 32 \times 64$ and $128 \times 32 \times 64$ ($AR = 1$), $64 \times 32 \times 128$ and $128 \times 32 \times 128$ ($AR = 2$), and $128 \times 32 \times 64$ and $256 \times 32 \times 64$ ($AR = 0.5$) elements inside and above the street canyon, respectively. The grid is stretched near the wall to better resolve the near-wall turbulence, and the minimum grid sizes are $5.319 \times 10^{-3}H$ in the streamwise and vertical directions and $3.125 \times 10^{-2}H$ in the spanwise direction. The grid is chosen based on a grid sensitivity test (Li et al. 2008), with the simulation time for the flow to reach pseudo-steady state being about $300H/U$. Another $300H/U$ simulation results were collected to retrieve the statistical flow, turbulence, and scalar properties with a timestep of $0.005H/U$.

## 3 Flow and Turbulence Fields

### 3.1 Mean Flow

Figures 2, 3, and 4 show the mean flow quantities of the street canyons under different ground-heating conditions. The streamfunction plot for the street canyon of $AR = 1$ (not shown here) exhibits a roughly symmetric pattern with corner vorticies and an impinging streamline on the windward wall near the canyon roof (Li et al. 2010). The streamfunctions increase in magnitude with increasing ground-heating intensities. For the deep street canyons of $AR = 2$ with no buoyancy forcing there are two large counter-rotating vortices, one above the other, with again three small corner vortices and an impinging streamline (Figs. 2a, 3d, 4d). The upper vortex is larger, stronger and obviously driving the vortex below. With weak heating at the ground in the street canyon there is a marked change in the vortices (Figs. 2b, 3e, 4e), with the bottom vortex becoming a little larger but considerably stronger. The buoyancy injected at the ground has obviously strengthened the adjacent vortex, which appears to be assisting in driving the upper vortex. With even greater heating there is only one dominant vortex with
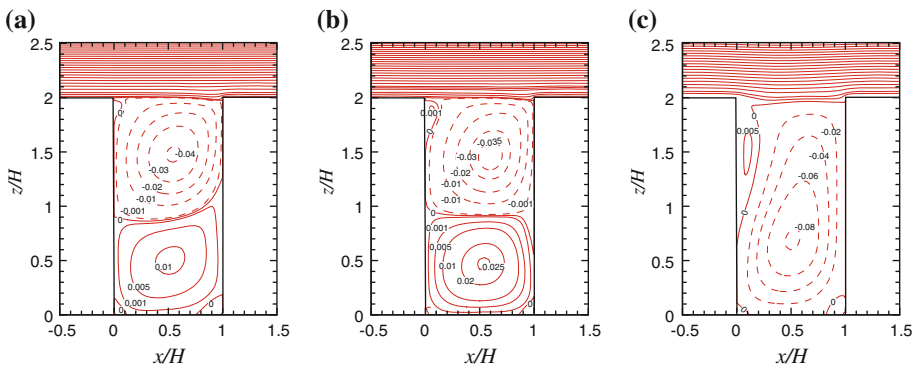


**Fig. 2** Spatial distribution of the dimensionless streamfunction $\psi$. in the street canyon of $AR = 2$. **a** Neutral; **b** weak heating; **c** strong heating. *Dashed lines* indicate negative values (clockwise rotating)
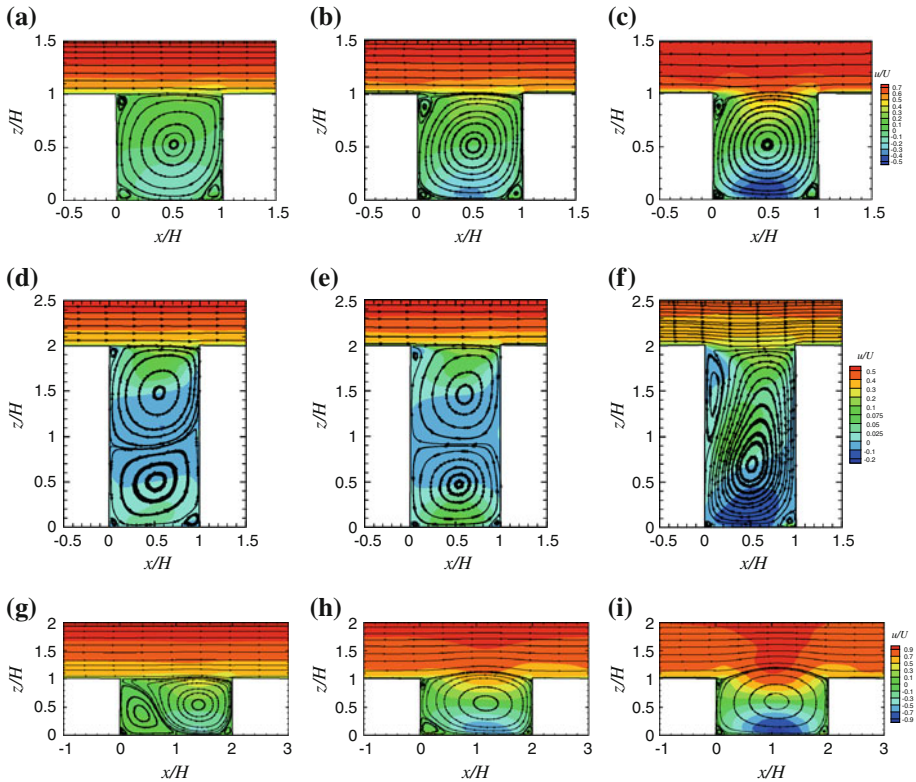
**Fig. 3** Flow patterns and normalized streamwise velocities $\langle \overline{u} \rangle / U$ in the street canyon of $AR = 1$ with **a** neutral, **b** weak, and **c** strong heating; in the street canyon of $AR = 2$ with **d** neutral, **e** weak, and **f** strong heating; in the street canyon of $AR = 0.5$ with **g** neutral, **h** weak, and **i** strong heating

its centre approximately 1/3 the way up the street canyon (Figs. 2c, 3f, 4f). The direction of rotation of this dominant vortex is that of the previous upper vortex and not that of the lower vortex that appeared to be increasing in strength with increased buoyancy injected from the ground. It seems that there is a fairly catastrophic change in the flow pattern at some critical condition. As can be seen in Fig. 2c. there are also three corner vortices and one of these, near the upper leeward wall, is of considerable size.

For the case of a wide street canyon of $AR = 0.5$ with no ground heating, Figs. 3g and 4g show two vortices aligned side by side. The downstream vortex is by far the larger and has the same sense of rotation as that in the street canyon of $AR = 1$. The upstream one is smaller but fills about 1/4 of the canyon and rotates in the opposite direction. Provision of a weak ground heating alters the flow drastically by changing the flow structure to a single dominant vortex with three small corner vortices and an impinging streamline near the windward roof. The great change in the streamline is undoubtedly due to the existing vortex sweeping the buoyant fluid back to the leeward wall where it rises, reinforcing the clockwise rotation; this is similar to the reinforcement seen in Figs. 3b, c and 4b, c for the street canyon of $AR = 1$. A strong ground heating produces an even stronger and more symmetric vortex, which extends even higher above the roof level. This is consistent with what Xie et al. (2007) calculated with a $k - \varepsilon$ model. Kim and Baik (2001), however, reported two counter-rotating vortices in a street canyon of $AR = 0.6$ with $\Delta \theta = 10 - 16$ K. It is evident that when buoyancy forces
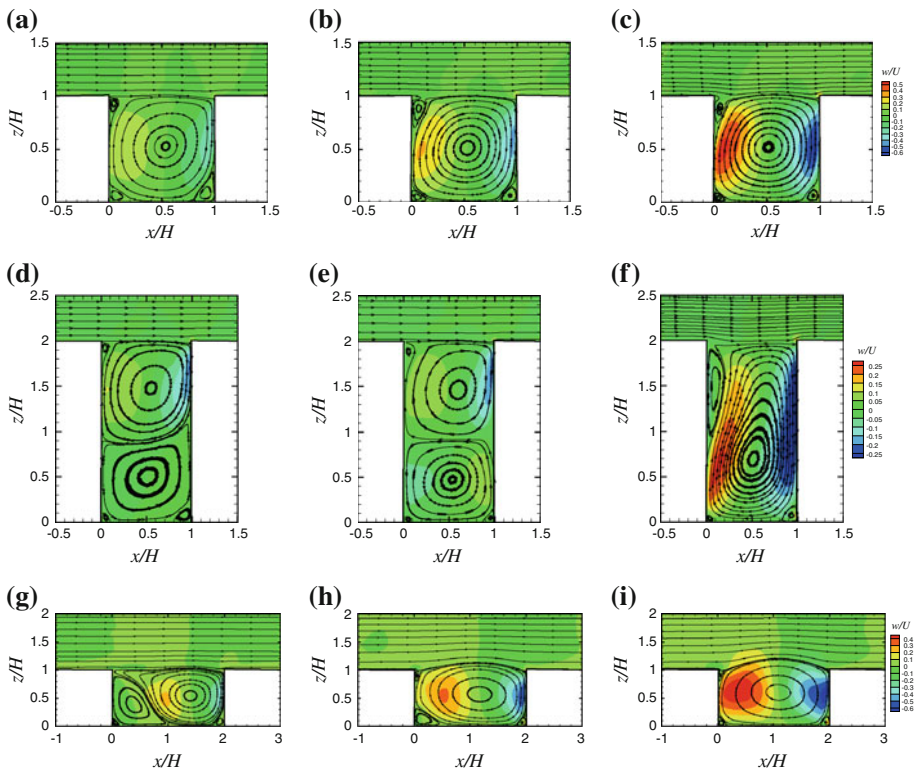
**Fig. 4** Flow patterns and normalized vertical velocities $\langle \overline{w} \rangle / U$ in the street canyon of $AR = 1$ with **a** neutral, **b** weak, and **c** strong heating; in the street canyon of $AR = 2$ with **d** neutral, **e** weak, and **f** strong heating; in the street canyon of $AR = 0.5$ with **g** neutral, **h** weak, and **i** strong heating

are introduced, the flow regime in the street canyon of $AR = 0.5$ changes from the WIF to the SF regime, although the SF regime here is somewhat different from the classical definition (e.g., in Oke 1988) in that the vortex extends above the street canyon to strongly disturb the free-stream flow, which does not happen in the street canyons of $AR = 1$ and 2. The coupling of the mean flow inside and above the street canyon suggests that the mean flow also contributes to the pollutant removal, which will be confirmed in the upcoming sections.

In all cases the buoyancy introduced at the ground in the street canyon acts to increase the magnitude of the velocity within the canyon, in addition to changing the flow structure markedly in some situations. This is clearly seen in Fig. 4. In the street canyon of $AR = 1$, the vertical velocity field is more organized on the windward side, the region where the free-stream fluid is first entrained into the canyon. It becomes less organized and more diffusive as the air moves around the street canyon. However, with increasing buoyancy at the ground the updraft on the leeward side becomes more organized and comparable to the downdraft on the windward side (Fig. 4a–c).

In the street canyon of $AR = 2$ this is even more marked, particularly with strong heating (Figs. 3f, 4f). The buoyant upflow and ingested downflow are very strong. Based on the principle of mass conservation, there must be a general equality of upflow and downflow, but their strengths have been equally affected by the buoyancy forces.

**Table 2** The combined effect of street canyon geometry (aspect ratio) and ground-heating intensities

*SF* skimming flow, *WIF* wake interference flow

| AR | Heating | | |
|---|---|---|---|
| | Neutral | Weak | Strong |
| 0.5 | WIF; two vortices | SF; one vortex | SF; one vortex |
| 1 | SF; one vortex | SF; one vortex | SF; one vortex |
| 2 | SF; two vortices | SF; two vortices | SF; one vortex |

Similar observations can be made for the street canyon of $AR = 0.5$, but they are even more striking (Figs. 3g–i, 4g–i). As the ground heating is intensified, the streamwise velocities inside the street canyon increase markedly and, somewhat surprisingly, the streamline pattern becomes strongly symmetric. For the vertical velocities, the symmetry is not quite as apparent but is still unusual. Additionally, with strong heating, the peak vertical velocities are about half the magnitude of the free-stream velocity, while the peak streamwise velocities are about the same in magnitude as the free-stream velocity.

The combined effect of geometry and heating discussed above is schematically summarized in Table 2.

### 3.2 Momentum Flux

The momentum fluxes $\langle u''w'' \rangle / U^2$ at the top of the street canyon represent the mixing between the freestream flow and the flow inside the street canyon. They reflect the transport of mass, momentum, sensible and latent heat and various air pollutants to or from the canyon and they are important in many urban studies. In Fig. 5a–c for the street canyon with $AR = 1$, the momentum flux into the street canyon (or the exchange velocity at the canyon roof level) increases by a factor of about 4 as the buoyancy is increased. It is also important to note that the momentum fluxes are very small within the street canyon when compared to those at the roof level. Much the same is seen in the results for $AR = 2$ (Fig. 5d–f). A slightly surprising observation is that, with strong heating (Fig. 5f), there is an organized pattern of Reynolds stresses within the canyon of considerable magnitude, and is likely the outcome of the strong organized flow in the canyon in this case.

The case of $AR = 2$ has the lowest momentum flux and the case of $AR = 0.5$ has the highest, where it is apparent that the lower $AR$ value allows for greater instability and mixing at the interface. For all aspect ratios the introduction of ground heating produces greater mixing across the canyon top as evidenced by the larger momentum fluxes.

## 4 Scalar Fields

### 4.1 Temperature

#### 4.1.1 Mean Temperature Difference

In the street canyon with $AR = 1$ (Fig. 6a, b), it is clear that most of the air in the street canyon is well mixed (or that, while the non-dimensional temperature difference $(\langle \overline{\theta} \rangle - \theta_a)/\Delta\theta$ varies from 0 to 1.0, most of the canyon is bounded by values that are only a small fraction of the temperature difference between the ground and the ambient temperature, with a typical value of 0.10). This small magnitude indicates that the exchange across the canyon top is relatively large compared to the surface heat transfer at the ground in the street canyon.
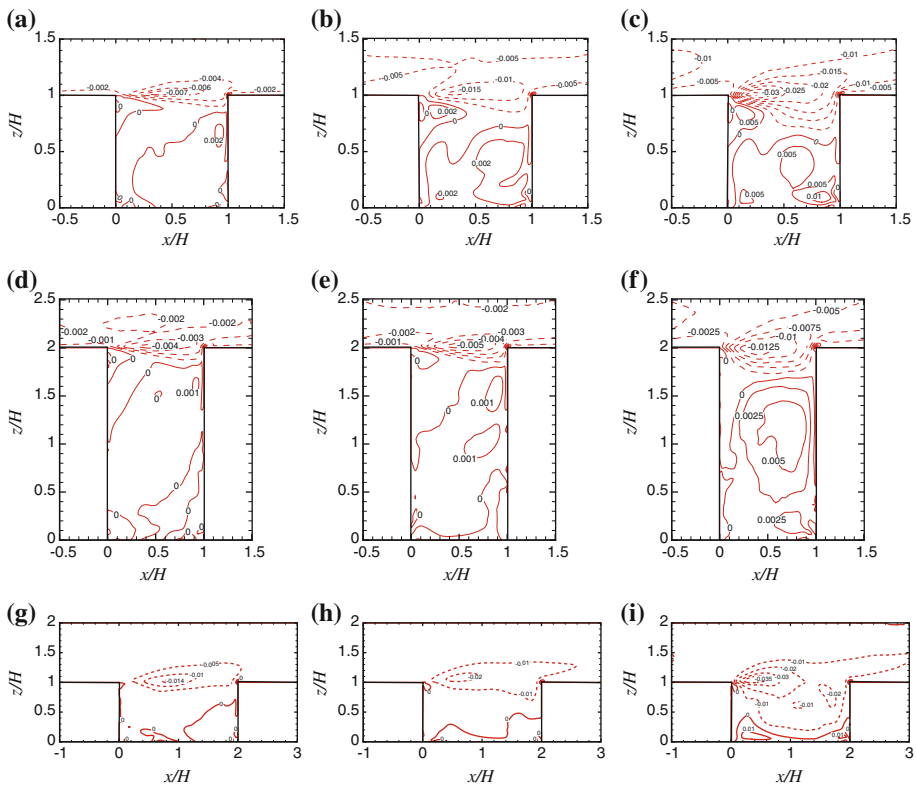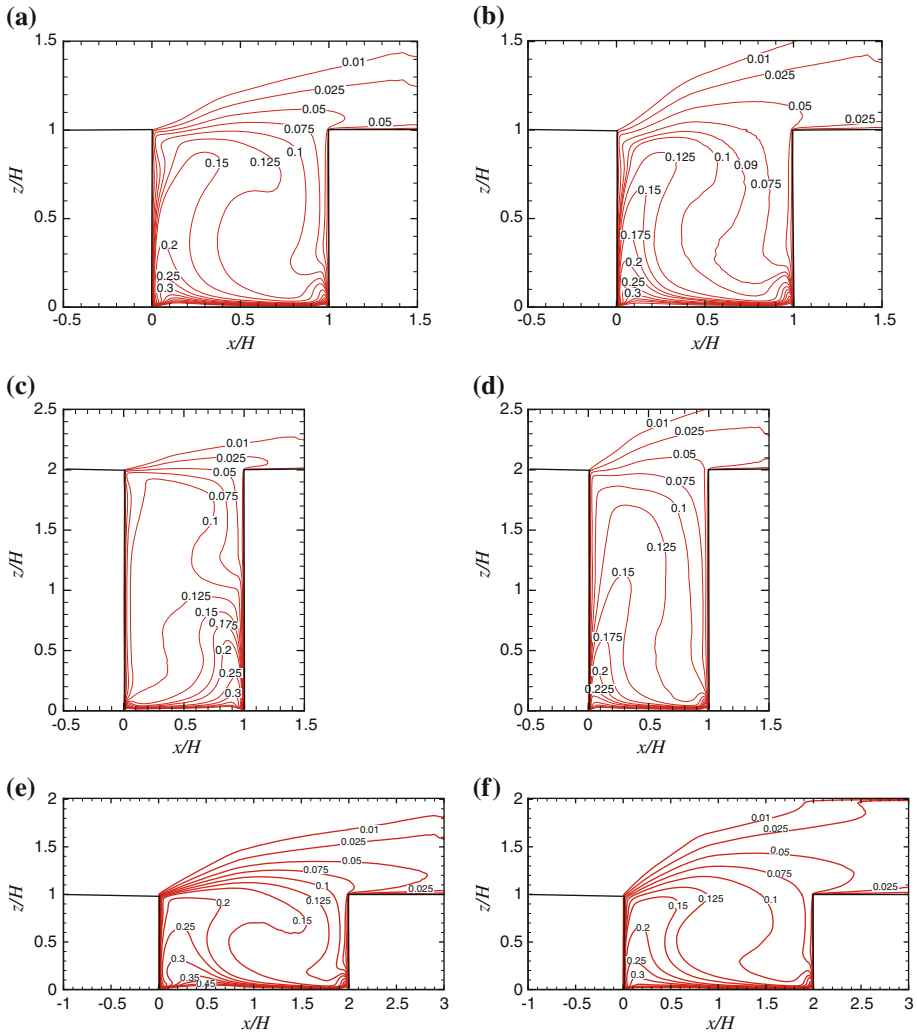
**Fig. 5** Normalized momentum flux $\langle u''w''\rangle/U^2$ in the street canyon of $AR = 1$ with **a** neutral, **b** weak, and **c** strong heating; in the street canyon of $AR = 2$ with **d** neutral, **e** weak, and **f** strong heating; in the street canyon of $AR = 0.5$ with **g** neutral, **h** weak, and **i** strong heating. *Solid lines* represent positive values while *dashed lines* represent negative values

Additionally the thermal plume above the street canyon not surprisingly extends higher into the free stream for the case with strong heating (Fig. 6b).

For the case of $AR = 2$ (Fig. 6c, d) the effect of increased ground heating is more complex in that the two-vortex structure is transformed into a single-vortex structure. However, for both heating cases the mixing as defined above is much the same. With the strong ground heating, in accordance with the dramatic flow pattern change, the leeward corner becomes warmer than the windward corner (Fig. 6d), contrary to the situation when only weak heating is present (Fig. 6c).

Much the same mixing of heat is observed in the street canyon with $AR = 0.5$ (Fig. 6e, f). Overall the mixing of heat within the street canyon is strong and somewhat insensitive to the aspect ratio (0.5–2) and heating intensity, the latter varying between small (down to zero) and quite strong (with a Richardson number $Ri$ up to $-2.9$). The numerical studies of Solazzo and Britter (2007) suggested that the flow and turbulence developed within the street canyon produced a temperature distribution that was essentially spatially uniform (apart from a relatively thin near-wall thermal boundary layer). To test the sensitivity of the current model to the boundary conditions, a simulation for the street canyon of $AR = 2$ with adiabatic (no heat flux) walls and roofs was performed (Fig. 7). The in-canyon temperature difference

**Fig. 6** Normalized mean temperature difference $(\langle\overline{\theta}\rangle - \theta_a)/\Delta\theta$ in the street canyon of $AR = 1$ with **a** weak and **b** strong heating; in the street canyon of $AR = 2$ with **c** weak and **d** strong heating; in the street canyon of $AR = 0.5$ with **e** weak and **f** strong heating

(normalized) is about 0.225, which signifies the important effect of the thermal boundary conditions.

### 4.1.2 Heat Flux

The turbulent transfer of heat within and across the street canyon is crucial for the in-canyon temperature distribution. The non-dimensional vertical heat flux $\langle w''\theta''\rangle/(U\,\Delta\theta)$ is shown in Fig. 8. In the street canyon with $AR = 1$ (Fig. 8a, b), there are local maxima at the leeward roof level and leeward and windward ground corners. It is clearly seen that heat circulates inside the street canyon at the core region, while substantial heat exchange occurs at the roof

**Fig. 7** The same as in Fig. 6c, but with adiabatic walls and roofs
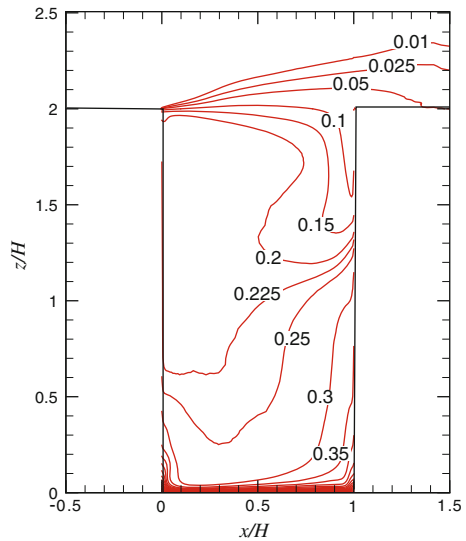


level. With strong ground heating (Fig. 8b), the heat exchange at the roof level is stronger, which explains the lower non-dimensional in-canyon temperature difference in the previous section (Fig. 6b).

In the street canyon with $AR = 2$ (Fig. 8c, d), the magnitude of heat fluxes is smaller than that in the street canyons of $AR = 1$ and 0.5, presumably due to the lower momentum flux observed in the previous section. Local maxima occur at the interface between vortices under both weak and strong heating conditions, suggesting large heat transfer due to turbulence. In contrast to the cases of $AR = 1$ and 0.5, the local maxima at the roof level are much lower than those at vortex interfaces and near the ground, implying that more heat accumulates and recirculates within the street canyon (Fig. 8d). The distribution of heat flux in the street canyon of $AR = 0.5$ (Fig. 8e, f) is similar to that in the street canyon of $AR = 1$, while the magnitude in the case of $AR = 0.5$ is slightly larger than that in $AR = 1$.

### 4.2 Pollutant Transport

#### 4.2.1 Mean Pollutant Distribution

As shown in Fig. 9, the general levels of non-dimensional pollutant concentrations $\langle \overline{c} \rangle U H L / Q$ vary quite considerably with changing aspect ratio and heating intensity at ground level. At the core region within the street canyons (where the pollutant distribution is quite uniform), the pollutant concentration changes from 45 to 20 to 12.5 for $AR = 1$, from 70 to 55 to 20 for $AR = 2$, and from 10 to 7.5 to 3.5 for $AR = 0.5$, with ground heating from neutral to weak to strong, respectively. Table 3 summarizes the pollutant ratio residing inside the street canyons for each case. The street canyon with $AR = 0.5$ is most effective in pollutant removal, and strong ground heating also plays an important role in this.

For the street canyon with $AR = 2$, when there is no heating or the ground heating is weak (Fig. 9d, e), the pollutant distribution exhibits two layers, roughly corresponding to the two layers within their streamlines. At the interface of these two layers, pollutant transport is solely through turbulent and molecular diffusion, which is relatively ineffective compared
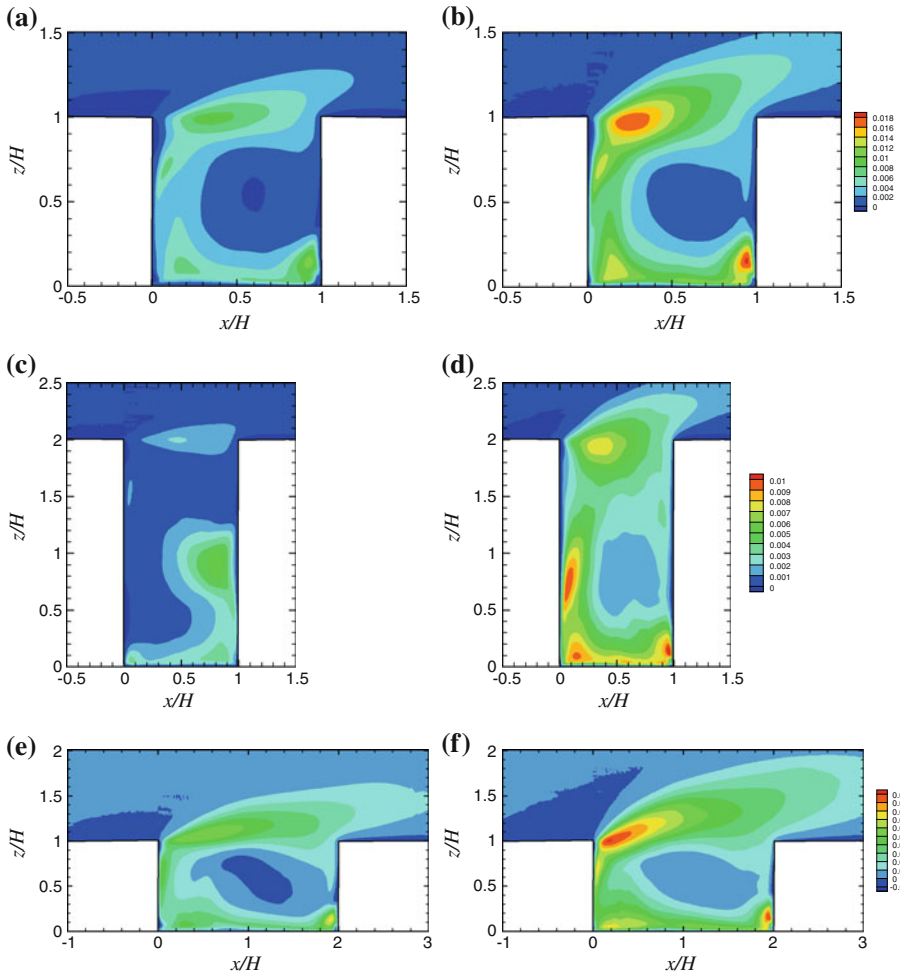
**Fig. 8** Normalized heat flux $\langle w''\theta''\rangle/(U\,\Delta\theta)$ in the street canyon of $AR = 1$ with **a** weak and **b** strong heating; in the street canyon of $AR = 2$ with **c** weak and **d** strong heating; in the street canyon of $AR = 0.5$ with **e** weak and **f** strong heating

with that by advection, resulting in the high accumulation of pollutants at the lower part of the street canyon and high pollutant retention inside the street canyon (Table 3). With the dramatic change in flow pattern when strong ground heating is present (Fig. 9f), the pollutant transport inside the street canyon by advection is more effective and the pollutant retention reduces from 97 to 93%, in contrast to the reduction from 98 to 97% for weak ground heating.

It is worth noting the difference between temperature and pollutant concentration, although they are both treated as scalars (one active and one passive) and governed by equations of the same form. The main reasons for their different distribution patterns are twofold. On the one hand, the source sizes are obviously different: temperature has an area heat source occupying the whole street floor, while the pollutant source is a line source situated in the middle of the street floor. Smaller sources are known to produce more detail in the concentration field (Fackrell and Robins 1982). On the other hand, the boundary conditions for each
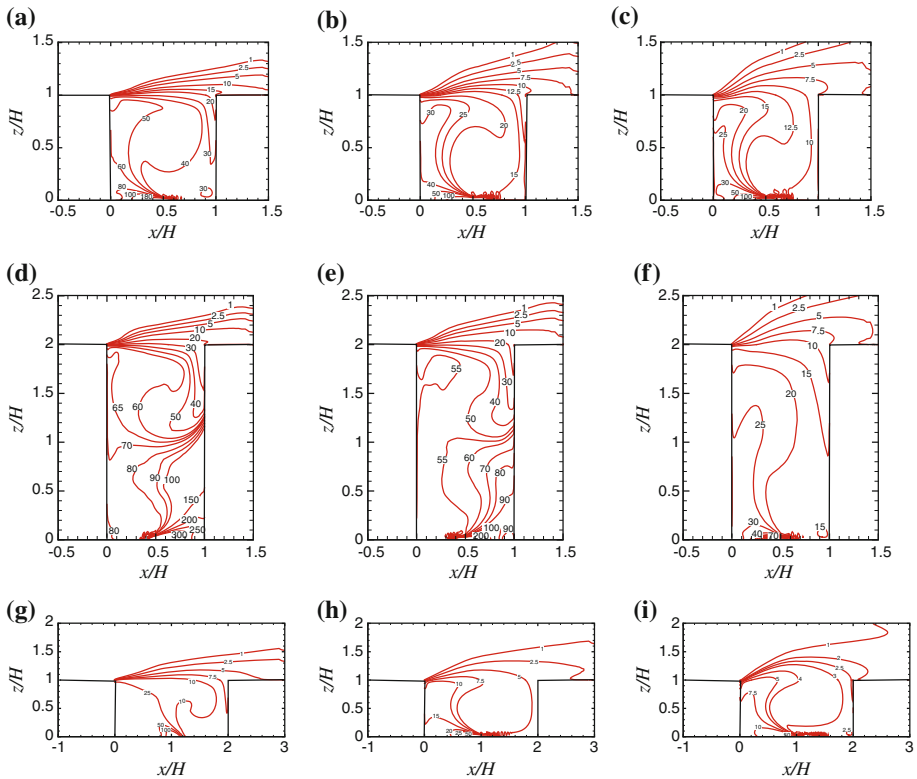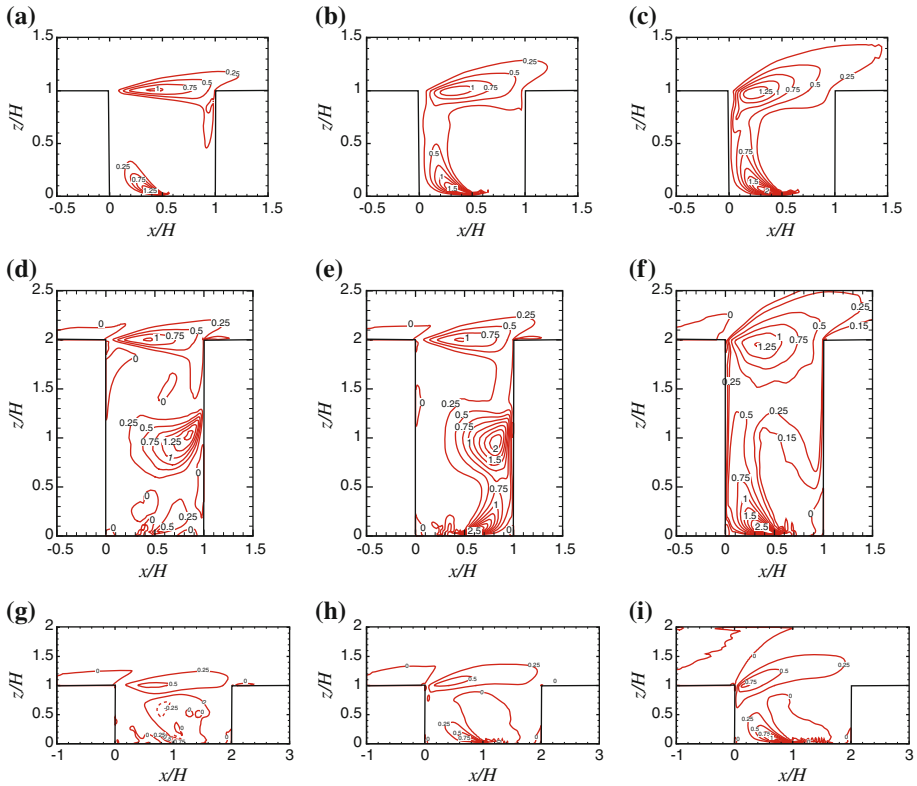
**Fig. 9** Normalized pollutant concentration $\langle \overline{c} \rangle UHL/Q$ in the street canyon of $AR = 1$ with **a** neutral, **b** weak, and **c** strong heating; in the street canyon of $AR = 2$ with **d** neutral, **e** weak, and **f** strong heating; in the street canyon of $AR = 0.5$ with **g** neutral, **h** weak, and **i** strong heating

**Table 3** Ratio of pollutants (%) inside the street canyon for different $AR$ values and with different ground-heating intensity

| AR | Heating | | |
|---|---|---|---|
| | Neutral | Weak | Strong |
| 0.5 | 90.7 | 80.5 | 72.5 |
| 1 | 93.6 | 89.3 | 83.6 |
| 2 | 97.8 | 97.0 | 92.7 |

scalar are different, as outlined in Sect. 2.2. Physically, heat transfer occurs at the solid walls, which are impermeable to pollutants. Mathematically, with the eddy-diffusivity assumption adopted in modeling the SGS heat (pollutant) fluxes, the governing equations are essentially elliptic. In addition, the temperature is fixed at most boundaries, therefore the temperature distribution must be basically fixed and independent of the heating intensity, and any slight variations in the temperature distribution are due to the differences in advection (Li et al. 2010). In contrast, the boundary conditions for the pollutant are mostly zero flux and hence the pollutant distribution is rather sensitive to the aspect ratio and heating intensity.

**Fig. 10** Normalized pollutant fluxes $\langle w''c'' \rangle (HL/Q)$ in the street canyon of $AR = 1$ with **a** neutral, **b** weak, and **c** strong heating; in the street canyon of $AR = 2$ with **d** neutral, **e** weak, and **f** strong heating; in the street canyon of $AR = 0.5$ with **g** neutral, **h** weak, and **i** strong heating

### 4.2.2 Pollutant Flux

To further examine how the buoyancy force enhances pollutant transport, the vertical pollutant fluxes $\langle w''c'' \rangle (HL/Q)$ for each case are depicted in Fig. 10 for comparison. In the street canyon with $AR = 1$ (Fig. 10a–c), the ground heating weakens the pollutant flux along the windward wall and, instead, strengthens the pollutant flux at the roof level, in the wake of the line source and along the leeward wall. This suggests that more pollutants are removed from the street canyon (through the roof-level leeward corner) while fewer are entrained inside (through the roof-level windward corner).

In the street canyon with $AR = 2$ (Fig. 10d–f), the pollutant flux is strengthened by weak ground heating in the wake of the line source and at the interface of two primary vortices. At the roof level, only a small magnitude of flux increment is found, and is in line with the negligible increment in pollutant removal by the weak ground heating, as noted in the previous section. With strong ground heating (Fig. 10f), the pollutant flux pattern somewhat resembles that in the street canyon with $AR = 1$ (Fig. 10c); high pollutant flux is observed near the ground leeward corner and the roof level.

For the street canyon with $AR = 0.5$ (Fig. 10g–i), the contour of the intensified pollutant flux due to the increasing ground heating does not cover the roof level as for the cases for

the other two aspect ratios described above. Instead, the contour of pollutant flux extends far above the roof level, which indicates that substantial pollutant exchange occurs above the roof level in this case. Hence, along the roof level, both mean flow and turbulence contribute to pollutant removal when ground heating is introduced, which conforms with Kang et al. (2008).

## 5 Conclusion

We employed a validated LES code to investigate the flow field and pollutant dispersion inside an urban street canyon of different aspect ratios with different ground-heating intensities. Neutral, weak, and strong heating cases for aspect ratios 1, 2, and 0.5 were studied to explore the combined effects of geometry and ground heating on the wind field and thermal environment, and pollutant dispersion, in urban areas.

It has been demonstrated that ground heating introduced in the street canyon strengthens the vortex motion. Of all the cases simulated, significant changes of flow and scalar patterns are caused by ground heating in the street canyons with $AR = 2$ and 0.5, while only the street canyon of $AR = 0.5$ shows a change in flow regime (from WIF to SF). Strong ground heating in the street canyon of $AR = 2$ can change the two-vortex structure into a one-vortex structure due essentially to the reinforced lower vortex. Strangely, the strong ground heating leads to a more symmetric vortex structure in the street canyons with $AR = 1$ and 0.5. Stronger ground heating produces greater mixing between the flow in the street canyon and that above, as reflected by larger momentum fluxes across the roof level of the street canyon. The mixing of heat in the street canyons of different aspect ratios is observed to be large. The normalized temperature differences inside the street canyon are spatially uniform and somewhat insensitive to the aspect ratio and the intensity of ground heating.

Generally, ground heating greatly facilitates pollutant removal for the street canyons at different aspect ratios. For the street canyon with $AR = 0.5$, when ground heating is introduced, substantial pollutant exchange occurs above the roof level, and mean flow as well as turbulence contributes to pollutant removal. The results obtained in this study can potentially benefit both the research community and urban planners who are concerned with urban thermal comfort.

## References

Ahmad K, Khare M, Chaudhry KK (2005) Wind tunnel simulation studies on dispersion at urban street canyons and intersections—a review. J Wind Eng Ind Aerodyn 93:697–717
Belcher SE (2005) Mixing and transport in urban areas. Phil Trans Roy Soc A 363:2947–2968
Blocken B, Stathopoulos T, Saathoff P, Wang X (2008) Numerical evaluation of pollutant dispersion in the built environment: comparisons between models and experiments. J Wind Eng Ind Aerodyn 96: 1817–1831
Bottema M (1993) Wind climate and urban geometry. Eindhoven University of Technology, Netherlands
Britter RE, Hanna SR (2003) Flow and dispersion in urban areas. Annu Rev Fluid Mech 35:469–496
Buccolieri R, Sandberg M, Di Sabatino S (2010) City breathability and its link to pollutant concentration distribution within urban-like geometries. Atmos Environ 44:1894–1903
Ca VT, Asaeda T, Ito M, Armfield S (1995) Characteristics of wind field in a street canyon. J Wind Eng Ind Aerodyn 57(1):63–80

Cai XM, Barlow JF, Belcher SE (2008) Dispersion and transfer of passive scalars in and above street can-
    yons—large-eddy simulations. Atmos Environ 42:5885–5895
Cheng WC, Liu CH (2011) Large-eddy simulation of turbulent transports in urban street canyons in different
    thermal stabilities. J Wind Eng Ind Aerodyn. doi:10.1016/j.jweia.2010.12.009
Cheng H, Hayden P, Robins AG, Castro IP (2007) Flow over cube arrays of different packing densities.
    J Wind Eng Ind Aerodyn 95:715–740
Cheng WC, Liu CH, Leung DYC (2009) On the correlation of air and pollutant exchange for street canyons
    in combined wind-buoyancy-driven flow. Atmos Environ 43:3682–3690
Coceal O, Thomas TG, Belcher SE (2007) Spatial variability of flow statistics within regular building arrays.
    Boundary-Layer Meteorol 125:537–552
Cui Z, Cai XM, Baker CJ (2004) Large eddy simulation of turbulent flow in a street canyon. Q J R Meteorol
    Soc 599:1373–1394
Fackrell JE, Robins AG (1982) The effects of source size on concentration fluctuations in plumes. Boundary-
    Layer Meteorol 22(3):335–350
Fernando HJS, Lee SM, Anderson J, Princevac M, Pardyjak E, Grossman-Clarke S (2001) Urban fluid mechan-
    ics: air circulation and contaminant dispersion in cities. Environ Fluid Mech 1:107–164
Hamlyn D, Hilderman T, Britter R (2007) A simple network approach to modelling dispersion among large
    groups of obstacles. Atmos Environ 41:5848–5862
Kang YS, Baik JJ, Kim JJ (2008) Further studies of flow and reactive pollutant dispersion in a street canyon
    with bottom heating. Atmos Environ 42:4964–4975
Kim JJ, Baik JJ (2001) Urban street-canyon flows with bottom heating. Atmos Environ 35:3395–3404
Letzel MO, Krane M, Raasch S (2008) High resolution urban large-eddy simulation studies from street canyon
    to neighbourhood scale. Atmos Environ 42:8770–9784
Li XX (2008) Large-eddy simulation of wind flow and air pollutant transport inside urban street canyons of
    different aspect ratios. PhD thesis, The University of Hong Kong, 205 pp
Li XX, Liu CH, Leung DYC, Lam KM (2006) Recent progress in CFD modelling of wind field and pollutant
    transport in street canyons. Atmos Environ 40(29):5640–5658
Li XX, Liu CH, Leung DYC (2008) Large-eddy simulation of flow and pollutant dispersion in urban street
    canyons with wall model. Boundary-Layer Meteorol 129(2):249–268
Li XX, Liu CH, Leung DYC (2009) Numerical investigation of pollutant transport characteristics inside deep
    urban street canyons. Atmos Environ 43(15):2410–2418
Li XX, Britter RE, Koh TY, Norford LK, Liu CH, Entekhabi D, Leung DYC (2010) Large-eddy simulation
    of flow and pollutant transport in urban street canyons with ground heating. Boundary-Layer Meteorol
    137(2):187–204. doi:10.1007/s10546-010-9534-8
Liu CH, Barth MC (2002) Large-eddy simulation of flow and scalar transport in a modeled street canyon.
    J Appl Meteorol 41(6):660–673
Liu CH, Barth MC, Leung DYC (2004) Large-eddy simulation of flow and pollutant transport in street canyons
    of different building-height-to-street-width ratios. J Appl Meteorol 43:1410–1424
Liu CH, Leung DYC, Barth MC (2005) On the prediction of air and pollutant exchange rates in street canyons
    of different aspect ratios using large-eddy simulation. Atmos Environ 39:1567–1574
Nakamura Y, Oke TR (1988) Wind, temperature, and stability conditions in an east-west-oriented urban
    canyon. Atmos Environ 22:2691–2700
Oke T (1988) Street design and urban canopy layer climate. Energy Build 11:103–113
Reynolds RT, Castro IP (2008) Measurements in an urban-type boundary layer. Exp Fluids 45:141–156
Sini JF, Anquetin S, Mestayer PG (1996) Pollutant dispersion and thermal effects in urban street canyons.
    Atmos Environ 30:2659–2677
Solazzo E, Britter RE (2007) Transfer processes in a simulated urban street canyon. Boundary-Layer Meteorol
    124(1):43–60
Uehara K, Murakami S, Oikawa S, Wakamatsu S (2000) Wind tunnel experiments on how thermal stratification
    affects flow in and above urban street canyons. Atmos Environ 34:1553–1562
Vardoulakis S, Fisher BEA, Pericleous K, Gonzalez-Flesca N (2003) Modelling air quality in street canyons:
    a review. Atmos Environ 37:155–182
Xie X, Huang Z, Wang J, Xie Z (2005) Thermal effects on vehicle emission dispersion in an urban street
    canyon. Transp Res D 10:197–212
Xie X, Liu CH, Leung DYC, Leung MKH (2006) Characteristics of air exchange in a street canyon with
    ground heating. Atmos Environ 40(33):6396–6409
Xie X, Liu CH, Leung DYC (2007) Impact of building facades and ground heating on wind flow and pollutant
    transport in street canyons. Atmos Environ 41:9030–9049
Yoshie R, Jiang G, Shirasawa T, Chung J (2011) CFD simulations of gas dispersion around high-rise building
    in non-isothermal boundary layer. J Wind Eng Ind Aerodyn. doi:10.1016/j.jweia.2011.01.006